Supporting Information to

Experimentally confirmed ferroelectricity in organic compounds identified by database mining

Maximilian Litterst[1], Manjunath Balagopalan[2], Ramon Jannasch[1], Elin Dypvik Sødahl[3], Seyedmojtaba Seyedraoufi[3], Carl Henrik Gørbitz[4], Kristian Berland[3], Ola Nilsen[2*], Martijn Kemerink[1,*]

[1] Institute for Molecular Systems Engineering and Advanced Materials, Heidelberg University, Im Neuenheimer Feld 225, 69120 Heidelberg, Germany

[2] Inorganic materials chemistry, Department of Chemistry, Norwegian University of Life Science, Oslo

[3] Department of Mechanical Engineering and Technology Management, Norwegian University of Life Sciences, 1432 Ås, Norway.

[4] Life Science, Department of Chemistry, Norwegian University of Life Science, Oslo

[*] Corresponding author. Email: ola.nilsen@kjemi.uio.no, martijn.kemerink@uni-heidelberg.de.

Contents

1 - IDE geometry considerations

Here, we provide a detailed explanation of the used IDEs and how to turn capacitance into permittivity, charge into polarization and the errors involved when screening for properties using IDE electrodes.

The measured electrical quantities are voltage, charge (integration of the current to time) and capacitance (measured with a lock-in amplifier). A first approximation for the electrical field is obtained by dividing the voltage by the gap of $5\ \mu m$. This value is only correct for the region directly between the electrodes (at the interface to the substrate). The electrical field will reduce when moving away

from the substrate [1]. Hence, our approximation of the electric field must therefore be considered an upper limit.

Normally, the property polarization is reported when working with ferroelectric materials, however, such is difficult to obtain directly when using IDEs and the equivalent of charge is rather reported. For the conversion of the charge to polarization, an area of $A = (2\,N\, - 1)Wh_{eff}$ is assumed. Here, N is the number of electrodes from each side, W their length and h_{eff} the effective height, which depends on the film thickness. $(2\,N\, - 1)W$ only depends on the electrode structure and equals $0.80\ m$ for the micrux IDE and $2.01\ m$ for the homemade one. Calculations based on Maxwell equations indicate that h_{eff} should be the film thickness, as long as the coercive field is reached across the entire film[1]. Geometric considerations assuming that the material is uniform often indicate that the field is sufficiently strong. The assumption of a uniform material is, however, not true in a ferroelectric material, as the permittivity strongly depends on the electric field and therefore the field is confined into the region where the coercive field is reached. Measurements with BTA [2] indicate that only the first 300-600 nm seem to be relevant for this material. Based on these measurements, the polarization can be calculated by $P = \frac{C}{A} = \frac{C}{2.013\ m*(300-600)\ nm}$. It is, however, not clear whether the same thickness can be assumed for the materials presented herein. For this reason, the total charges are not directly converted into a polarization for our work.

The conversion of capacitance to permittivity potentially suffers from the same problems and we keep to only report capacitance. For normal materials with permittivity ϵ_{mat} and thickness t on a substrate with permittivity ϵ_{sub}, the capacitance is given by $C = \frac{C_0}{2} * (1 + \epsilon_{sub} + (\epsilon_{mat} - 1) * F(t))$ [3]. $F(t)$ is a nonlinear function, that accounts for the decreasing influence of the upper layers and approaches unity for film thicknesses of about twice the electrode spacing. It is explicitly given in [3]. This is confirmed by 2d-periodic boundary finite element simulations with COMSOL Multiphysics as shown in Fig. S1.

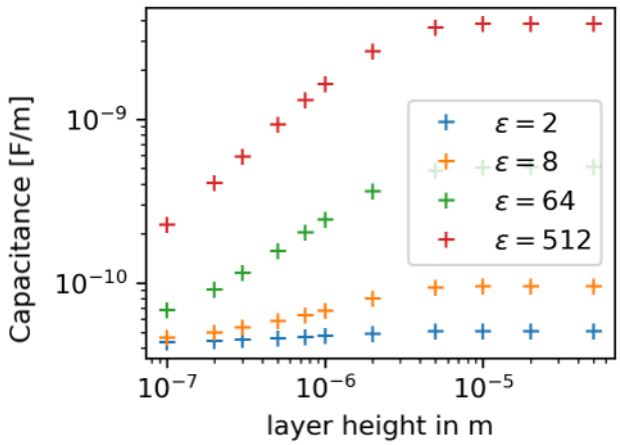

Fig. S1: Capacitance per unit length for different permittivites and layer thicknesses.

Finite-element simulations for the MicruX IDEs provide $C_0 = 10.2\ pF$ and measurements with an empty IDE give $\epsilon_{sub} = 4.5 \pm 0.5$ (error is variation between different substrates). With a known thickness, it becomes possible to convert the capacitance to a permittivity assuming that the permittivity is uniform across the material thickness.

If ferroelectric switching occurs, $F(t)$ changes to a function that depends on the material and is generally unknown. For this reason, the capacitance is provided and not converted to permittivity.

2 - Explanation of double wave method

The idea of the double wave method (DWM) is that there are two consecutive triangular voltage pulses in up- and down directions. For simplicity, only the first half is shown Fig. S2(a).

Both voltage pulses trigger the same non-hysteretic current responses like displacement currents (Fig. S2(a), orange), leakage currents (blue) or in case of a leaky dielectric, a combination of both (purple)). Hysteretic behavior will cause different currents in both voltage pulses. In case of a ferroelectric, this will be a current peak during the first increasing voltage slope, while there is no peak in the second, unless the material depolarizes between the pulses. This peak gets added onto the non-hysteretic currents, which is displayed in Fig. S2(a), brown. Other hysteretic phenomena will also cause different currents for both voltage waves. In case of ionic hysteresis this will by an displacive-like current ($I \propto dV/dt$) in the first wave[4], while slow dielectric relaxation will result in a rounding off and lagging behind of the displacement current. If the time between the pulses is too short for the relaxation to occur, the first wave might be affected more than the second. There is however no other phenomenon than ferroelectricity which will reliably produce a neat current peak, i.e. a peak with a maximum that sits before the maximum in driving voltage, in the first, but not the second voltage wave.

The current difference between the two voltage pulses is then calculated and integrated, as shown in Fig. S2(b). For ferroelectrics, this results in a saturating (flattening above the coercive field) hysteresis curve, as displayed in Fig. S2(b), brown. Importantly, this difference only exists for hysteretic current contributions, so consequently all non-hysteretic currents will not contribute to the calculated hysteresis (Fig. S2(b), blue, orange and purple).

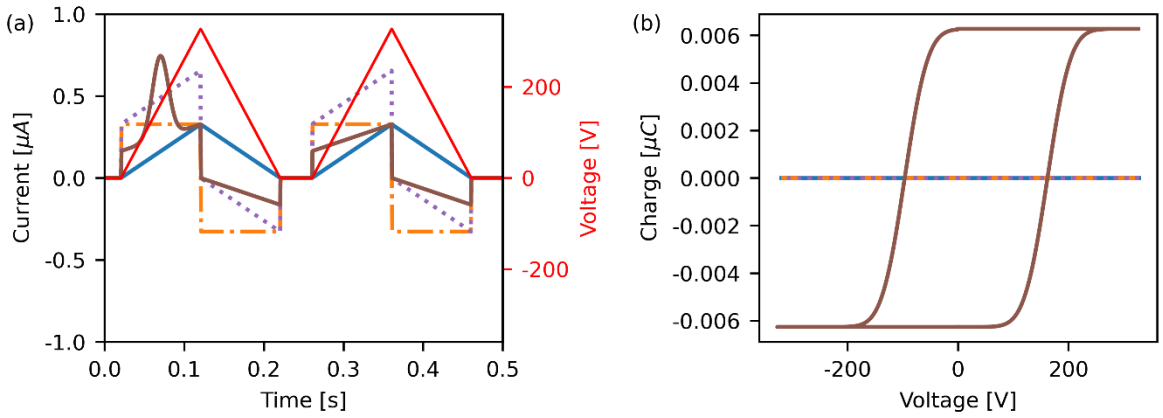

Fig. S2: (a) Currents responses of different samples to the first half of the DW signal: blue: resistor/material with background conductivity; orange: capacitor/dielectric material; purple: sum of blue and orange/leaky dielectric; brown: ferroelectric with notable background conductivity and dielectric contributions.

For the materials in this work, there were also minor ionic hysteresis contributions. On top of the ferroelectric switching peak (around 1.5 V) in SI Fig. S8a, the current at maximal voltage in the first wave is also a bit higher than in the second. This is assumed to be the ionic hysteresis that should not be represented in the ferroelectric hysteresis curve. To avoid including this charge for the ferroelectric charge, the current of the second wave is rescaled so that its maximum is at the same height as the first.

The integrated curves often showed a minor asymmetry leading to open hysteresis curves. This is probably due to some asymmetry of the device or due to the presence of trapped charges and not of the underlying material. To achieve closed hysteresis loops that have only one remnant polarization, both sides of the hysteresis curves are rescaled to the mean of the remnant polarizations.

The rescaling of the currents and its effects on the hysteresis can be seen in Figs. S7a, b.

The hysteresis curves of UHUMEP were measured with another setup, where the current detector had a low resolution. For this reason, the current was smoothed before applying the previously described steps. The raw and final data can be seen in Fig. S15a,b.

Explanation of sharp edges in the polarization hysteresis curves at $V = 0$

For the hysteresis curves shown in Figs. S7,8 and S11, as well as in Figs. 3-5 of the main text, there appear sharp edges at 0V. This is an artefact of the missing flat space between the two voltage pulses. The core assumption of the DWM is that both voltage waves induce mostly the same currents, with only the ferroelectric switching current being different. While this is mostly true, there are deviations in the first couple of datapoints due to the different voltage history: the first wave of any pair starts from opposite voltage, thus having one (positive for the first of the two positive waves) displacement current, while the second wave starts from the same voltage and thus the opposite (negative for the second of the two positive waves) displacement current. This can, e.g., be seen by the blue and orange curves in Fig. S4 having different starting currents at 0V, resulting in a noticeable difference (green). This is shown in more detail in Fig. S3 where each datapoint is shown individually. The same effect does not occur for the end of the voltage wave, where there has been the same history, resulting in the same current and therefore the difference (green) being very close to 0. The (green) difference curves of the two parts are combined and integrated for the hysteresis curve, resulting in the kink at 0V. Importantly, this does not significantly affect the overall shape and magnitude of the PE-loops - coercive fields and (saturating) remnant polarizations are (within experimental error) unaffected.

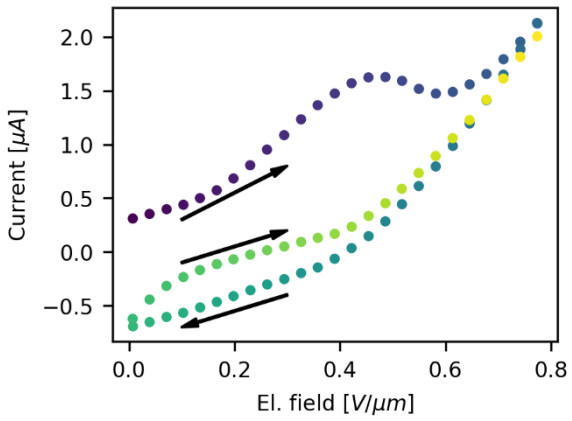

Fig. S3: Current vs. electric field for the double wave measurement of material 1 at 25 mHz (same data as Fig. S8)

3 - Modification to C(V)-loops

It was noted that the capacitance of most measured C(V)-loops decreases slightly within the measurement. As there is no physical reason for any asymmetry within the measurement and the decrease always happens over the measurement time, the most likely explanation for this is a change in the material like Joule heating or material degradation. To compensate for this, the curves are rescaled according to the following procedure, all the raw data is shown below:

The first, last and middle data point all correspond to a voltage of 0 V. The capacitance at these points is averaged (mean 0 V). Each datapoint is then rescaled by a factor that linearly changes from the factor

that rescales the first datapoint, to the one rescaling the middle datapoint, to rescaling the last datapoint.

4 - Data empty IDEs

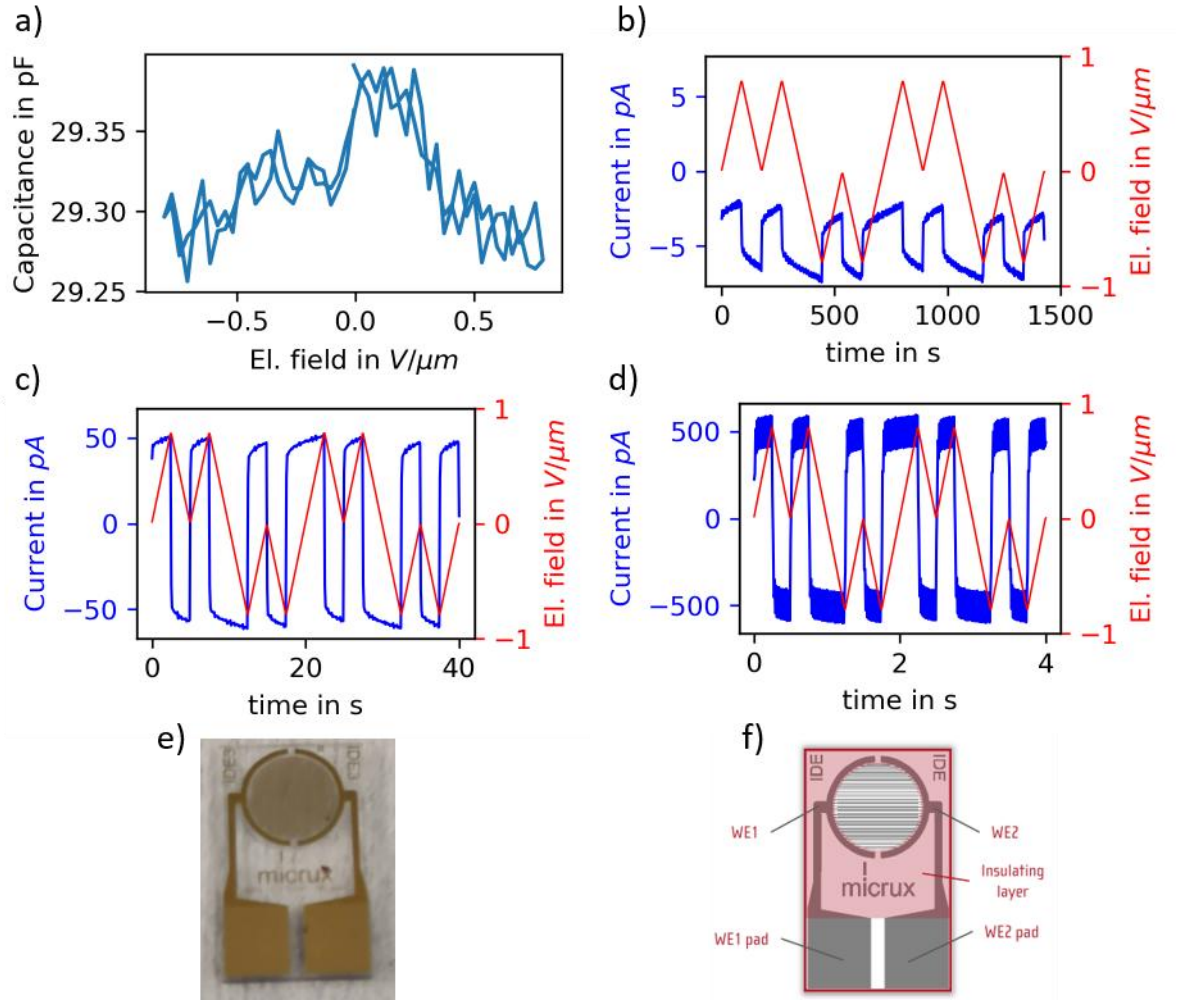

Fig. S4: a) CV of an empty MicruX IDE, b-d) Current response to the DWM Voltage at b) 0.7mHz, c) 25mHZ and d) 250mHz; The current sensor has an offset of about 4pA, e) photo of the empty IDE, f) sketch of an IDE, taken from micruxfluidic.com.

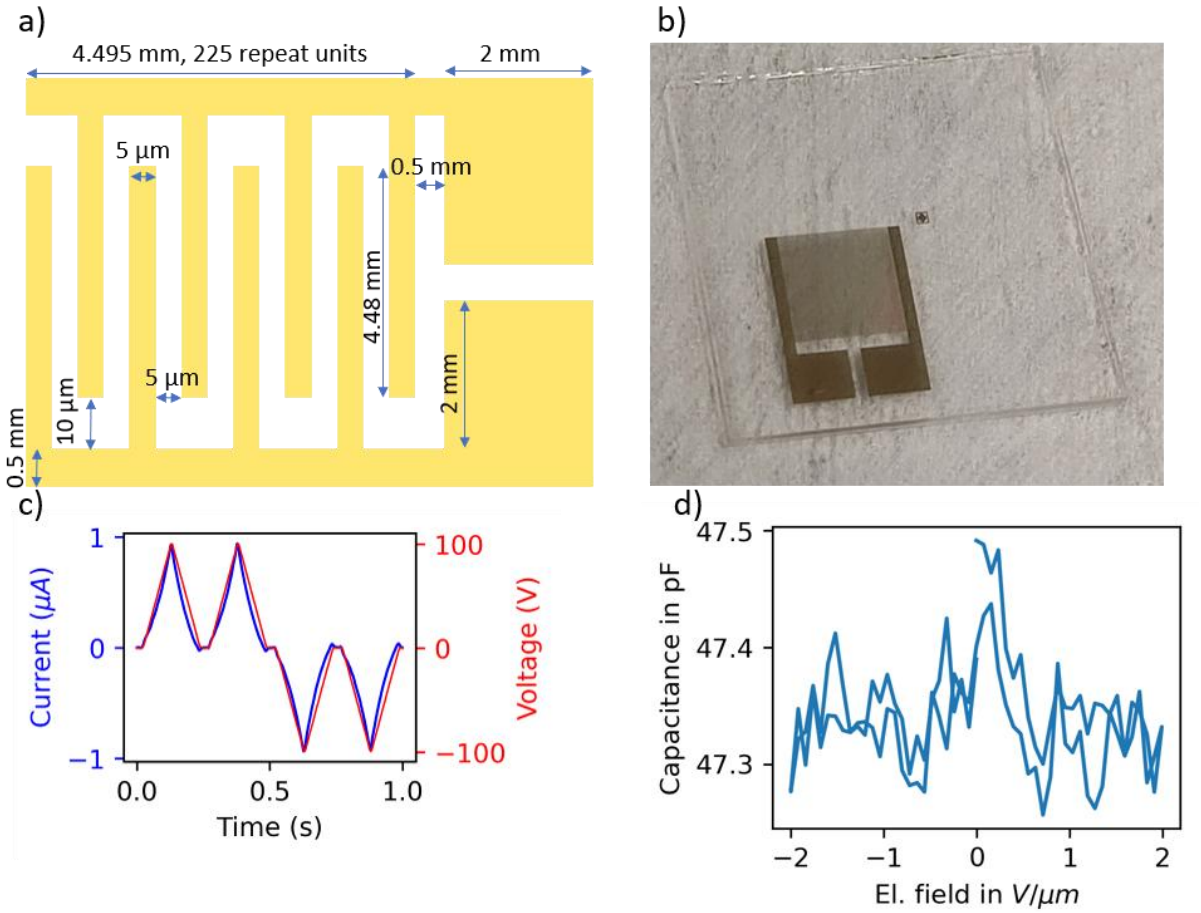

Fig. S5: a) sketch of a homemade IDE, b) photo of the real IDE, c) its DW and d) its C(V) signal

5 - Microscope images of finished samples

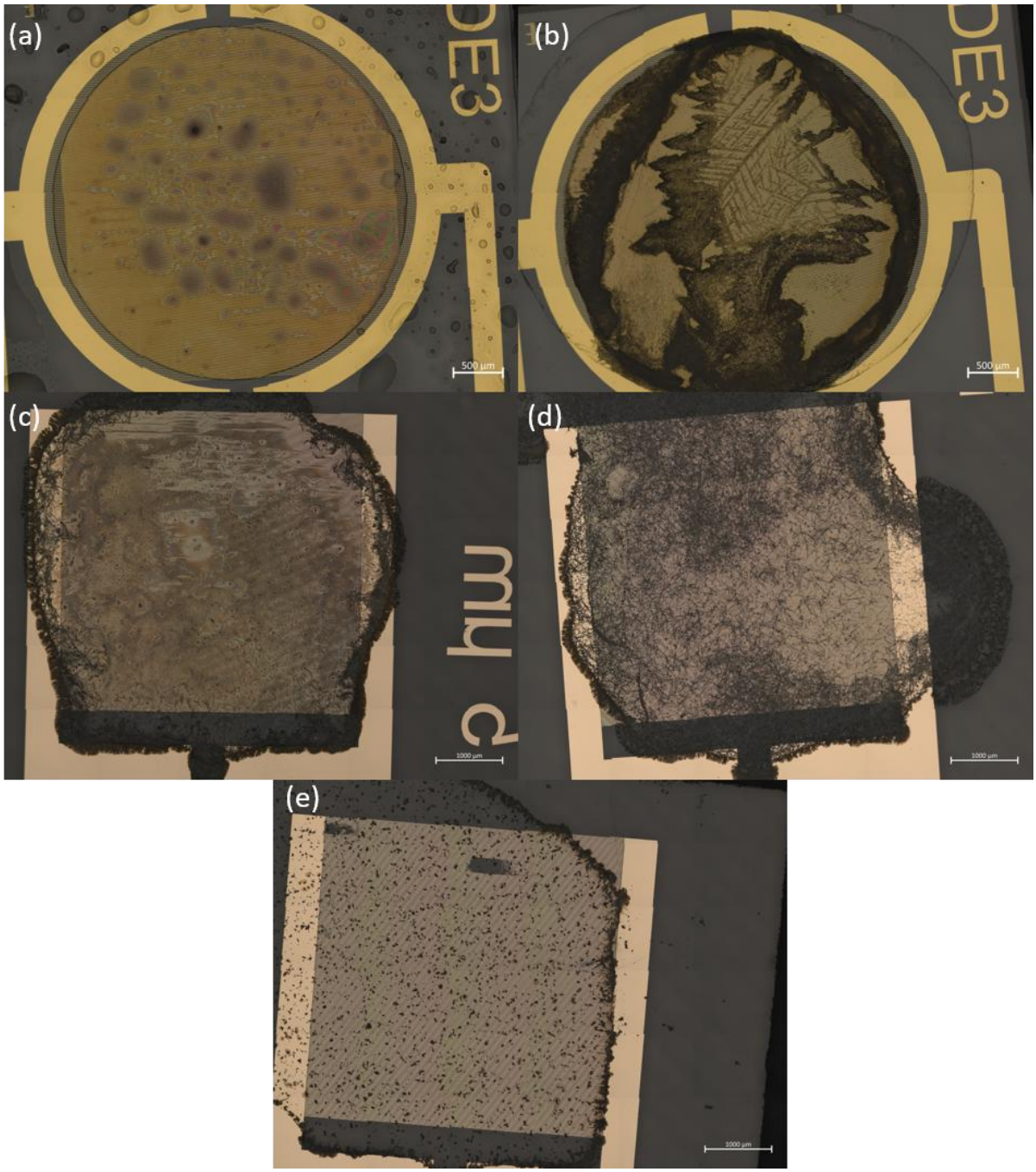

Fig. S6: Optical microscope images of the samples in this work: (a) **material 1**;(b) **material 2**; (c) ferroelectric sample of **material 4**; (d) inactive sample of **material 4**; (e) sample of **material 4** with unclear electronic behavior. The sample of **material 1** was already old when the image was taken, which is why only traces of the material remain on the IDE. The scale bar of (a) and (b) is 500 µm, for (c)-(e) it is 1000 µm.

6 - Data for TOZTAF

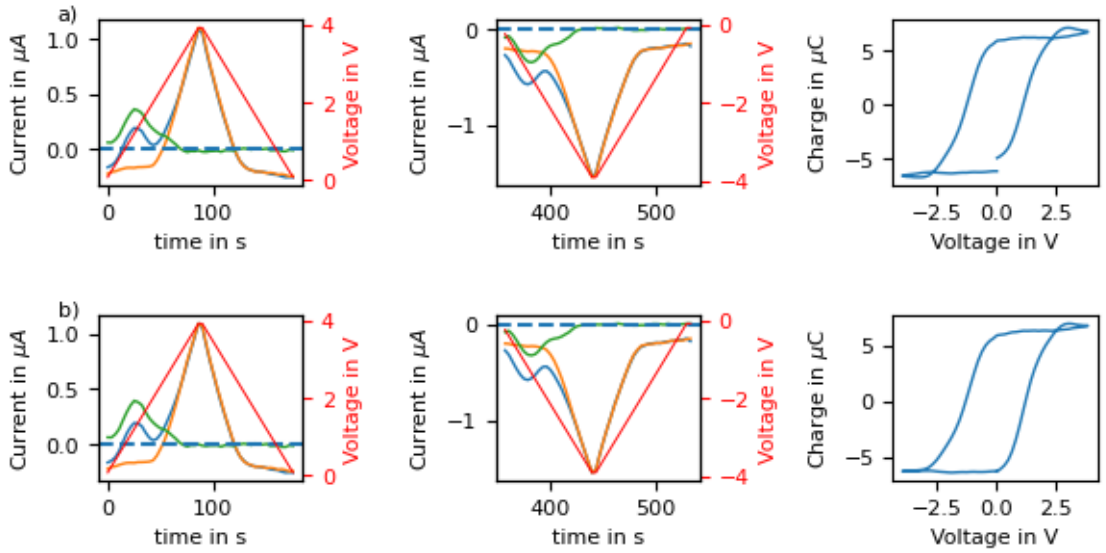

Fig. S7: a) raw data for TOZTAF, measured az 0.7 mHz, evaluated to the original double wave method [5], b) data modified according to SI section 2; As a) shows the raw data, the voltage is shown, while for b), the voltage is converted to the electric field (see SI section 1); the blue curve shows the current in the first voltage pulse, the orange the current in the second voltage pulse and orange the difference between thw two. Red shows the applied voltage.

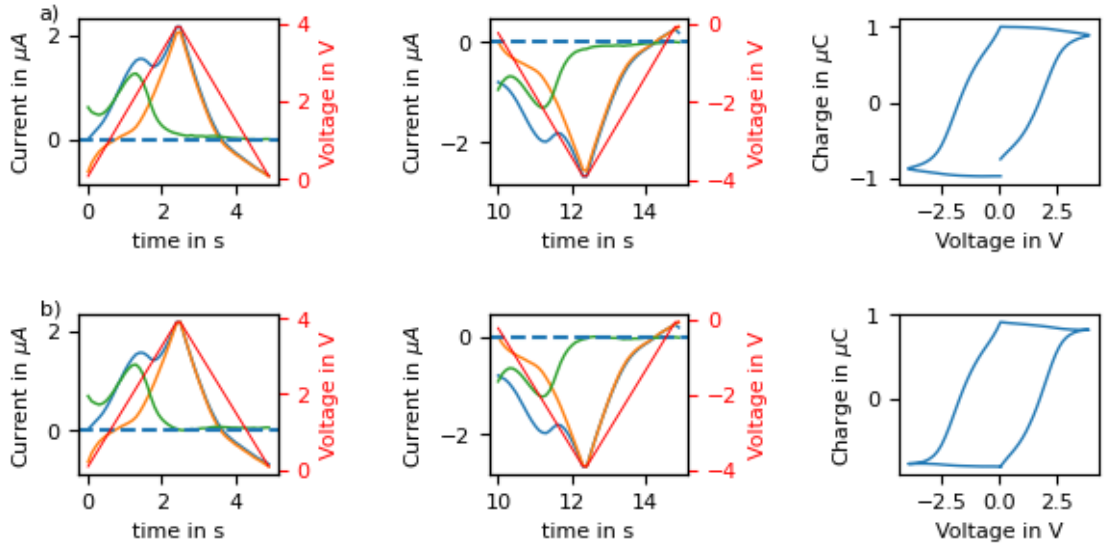

Fig. S8: a) raw data for TOZTAF, measured az 25 mHz, b) data modified according our evaluation method (SI section 2), same color coding as Fig. S3.

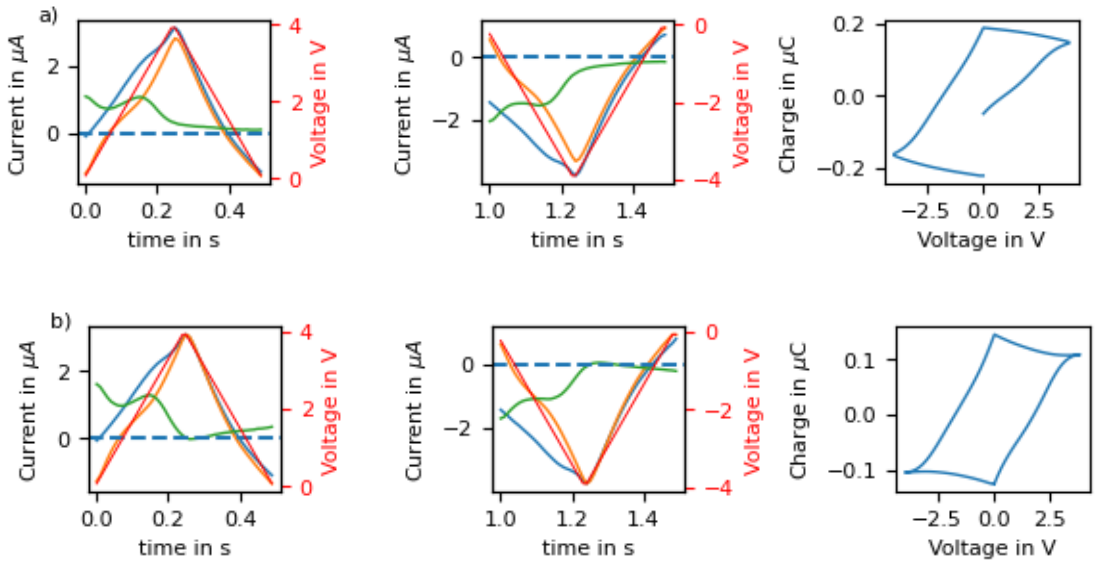

Fig. S9 a) raw data for TOZTAF, measured az 250 mHz, b) data modified according our evaluation method (SI section 2), same color coding as Fig. S3.

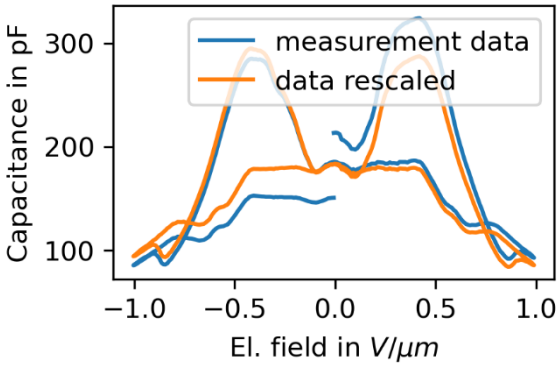

Fig. S10: C(V) measurement for TOZTAF, raw data in orange, blue shows the data rescaled according to SI section 3

7 - Data for HMTAAB

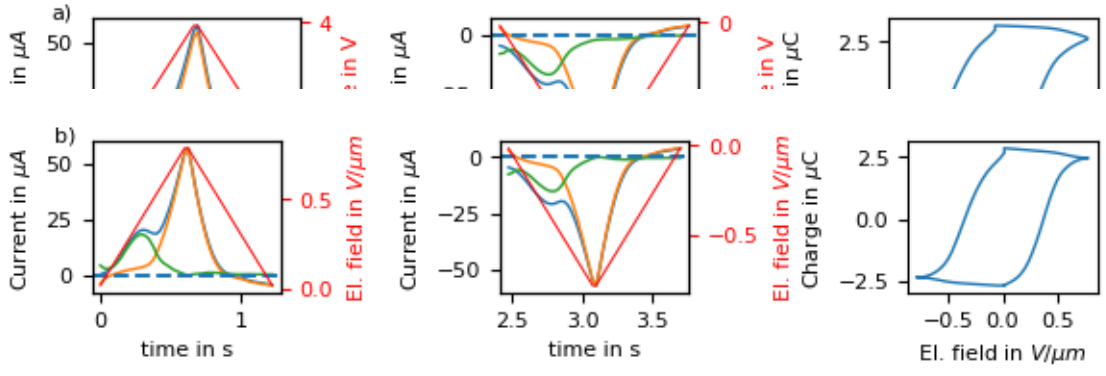

Fig. S11: a) raw data for HMTAAB, measured az 100 mHz, b) data modified according our evaluation method (SI section 2), same color coding as Fig. S3.

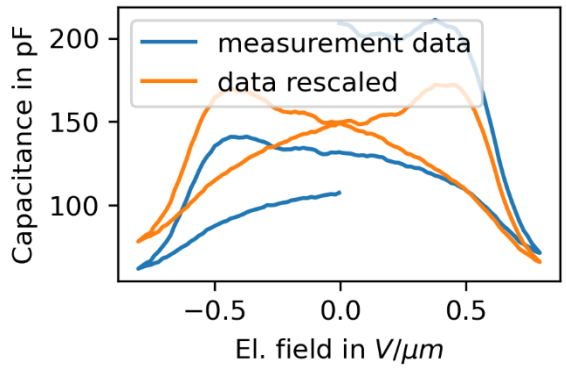

Fig. S12: C(V) measurement for HMTAAB, raw data in orange, blue shows the data rescaled according to SI section 3

8 - Data ZZZVPE

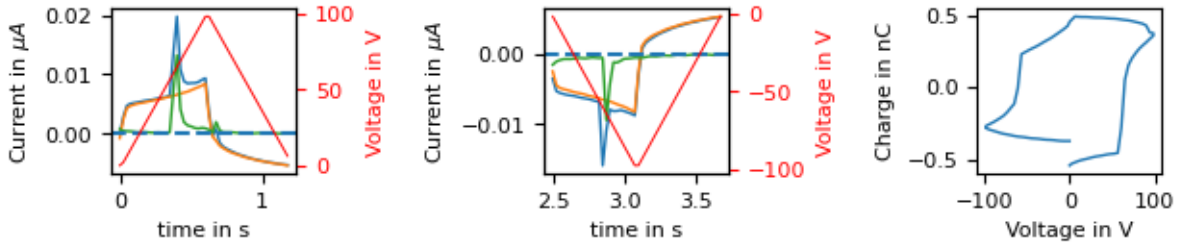

Fig. S13: raw data for ZZZVPE, measured az 100 mHz, the data is not evaluted according to (SI section 2) as it the curve is not that of a typical ferroelectric, same color coding as Fig. S3.

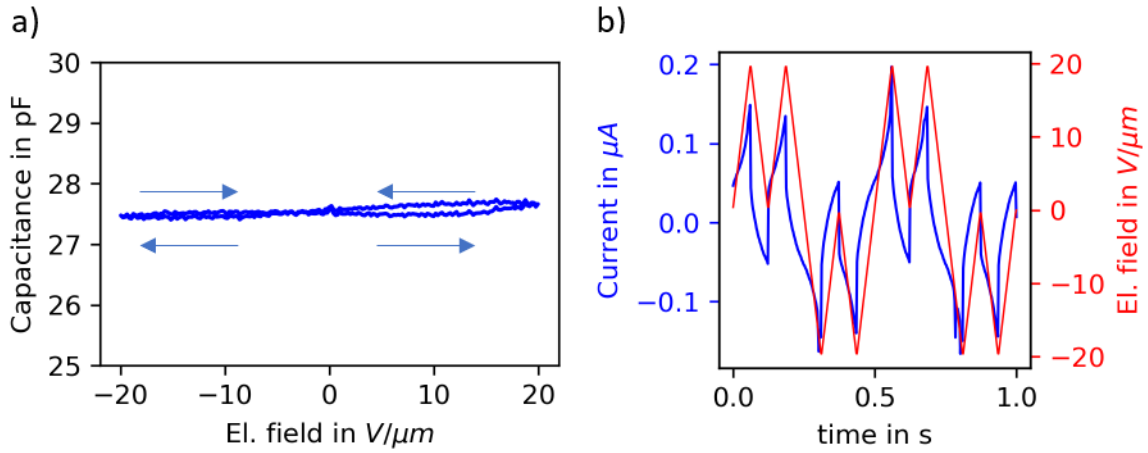

Fig. S14: a) Raw C(V) measurement for ZZZVPE (same sample as in SI Fig.13), arrows indicate the measurement direction, b) other sample, showing similar peaks in DW measurement.

9 - Data for UHUMEP

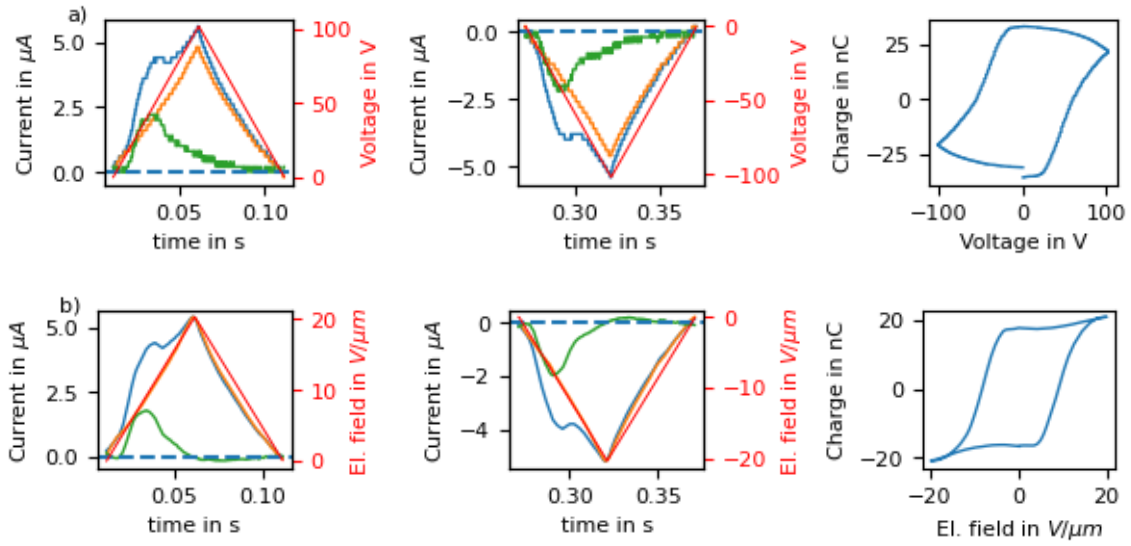

Fig. S15: a) raw data for UHUMEP, measured az 2 Hz, b) data modified according our evaluation method (SI section 2) and smoothed, same color coding as Fig. S3.

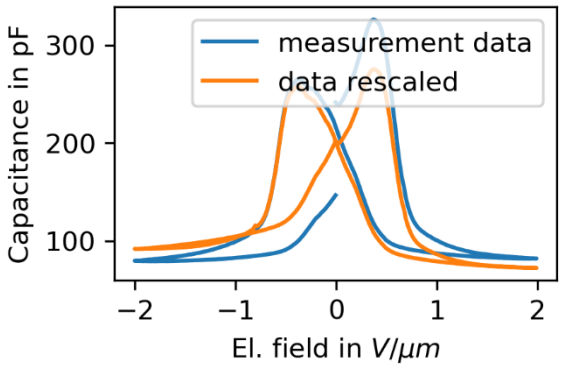

Fig. S16: C(V) measurement for a) normal behaving and b) unusually behaving UHUMEP, raw data in orange, blue shows the data rescaled according to SI section 3

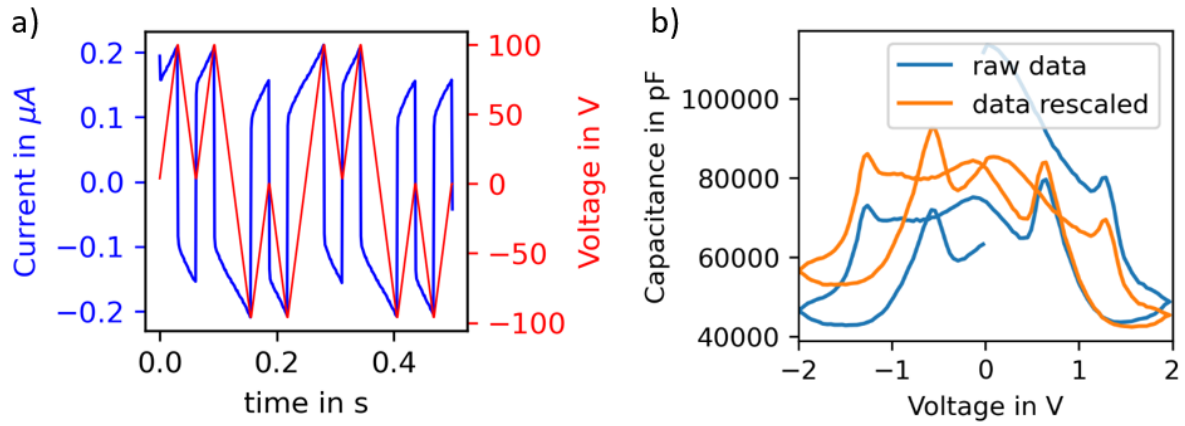

Fig. S17: a) DWM and b) C(V) measurement of strangely behaving UHUMEP sample

10 - Supplementary references

[1] R. Nigon, T. M. Raeder, and P. Muralt, "Characterization methodology for lead zirconate titanate thin films with interdigitated electrode structures," *J. Appl. Phys.*, vol. 121, no. 20, p. 14, May 2017, doi: 10.1063/1.4983772/153690.

[2] I. Urbanaviciute *et al.*, "Suppressing depolarization by tail substitution in an organic supramolecular ferroelectric," *Phys. Chem. Chem. Phys.*, vol. 21, no. 4, pp. 2069–2079, Jan. 2019, doi: 10.1039/C8CP06315J.

[3] N. J. Kidner, A. Meier, Z. J. Homrighaus, B. W. Wessels, T. O. Mason, and E. J. Garboczi, "Complex electrical (impedance/dielectric) properties of electroceramic thin films by impedance spectroscopy with interdigital electrodes," *Thin Solid Films*, vol. 515, no. 11, pp. 4588–4595, Apr. 2007, doi: 10.1016/J.TSF.2006.11.038.

[4] D. A. Jacobs *et al.*, "Hysteresis phenomena in perovskite solar cells: the many and varied effects of ionic accumulation," *Phys. Chem. Chem. Phys.*, vol. 19, no. 4, pp. 3094–3103, Jan. 2017, doi: 10.1039/C6CP06989D.

[5] M. Fukunaga and Y. Noda, "New Technique for Measuring Ferroelectric and Antiferroelectric Hysteresis Loops," *https://doi.org/10.1143/JPSJ.77.064706*, vol. 77, no. 6, May 2008, doi: 10.1143/JPSJ.77.064706.